Electrochemistry Communications 60 (2015) 199–203

Contents lists available at ScienceDirect

Electrochemistry Communications

journal homepage: www.elsevier.com/locate/elecom

Effect of hydrogenation on performance of TiO_2(B) nanowire for lithium ion capacitors

A. Byeon [a,b,1], M. Boota [a,1], M. Beidaghi [a,2], K.V. Aken [a], J.W. Lee [b,**], Y. Gogotsi [a,*]

[a] A. J. Drexel Nanomaterials Institute and Department of Materials Science and Engineering, Drexel University, Philadelphia, PA 19104, United States
[b] Department of Chemical and Biomolecular Engineering (BK-21 Plus), Korea Advanced Institute of Science and Technology, 291 Daehak-ro, Yuseong-gu, Daejeon 305-701, Republic of Korea

ARTICLE INFO

Article history:
Received 4 August 2015
Received in revised form 3 September 2015
Accepted 6 September 2015
Available online 15 September 2015

Keywords:
TiO_2(B)
Nanowire
Lithium ion capacitor
Hydrogenation
Pseudocapacitor

ABSTRACT

TiO_2(B) nanowires have shown excellent capacitance and energy density with a very low charge transfer resistance in 80-μm thick lithium ion capacitor electrodes. Nanowires hydrogenated by heat treatment at 500 °C showed improved Li ion diffusion and an increase in capacitance from 148 to 194 F/g as well as energy density from 23 to 30 Wh/kg. Hydrogenation of oxides as a way to improve their capacitance is critically discussed.

1. Introduction

Energy storage demand is increasing from portable electronics to the power grid. Supercapacitors are attractive as energy storage devices due to their high power density and good cyclability; however, the low energy density is the limiting factor. Energy density, *E*, can be increased mainly by two ways: 1) by increasing the capacitance, *C*, via design of high capacity electrodes beyond carbon and 2) by expanding the voltage window, *V*, of the devices ($E = 1/2\ CV^2$) [1]. Pseudocapacitive materials, such as metal oxides [2] or organic redox-active molecules [3], are commonly used to increase the charge storage capacity of the capacitive electrodes via additional redox processes at the electrode-electrolyte interface. One way to design high energy and power density devices is to use pseudocapacitive materials (high capacitance) in organic electrolytes (large voltage window). The concept of lithium-ion capacitor (LIC) provides high energy and power density by using a pseudocapacitive material as an anode and activated carbon as a cathode in an organic electrolyte [4]. LICs can accommodate both faradaic (lithium insertion/extraction) and non-faradaic (adsorption/desorption) processes at the same time with an expanded voltage window in lithium-based organic electrolytes [5].

Among various TiO_2 phases, TiO_2(B) bronze phase has gained attention as a lithium insertion material due to its high theoretical capacity of 335 mAh/g and good rate capability [6]. Compared to other TiO_2 phases involving bulk diffusion-controlled mechanism, TiO_2(B) has an open structure allowing faster lithium ion uptake. However, it still suffers from sluggish ionic transport and poor electronic conductivity. To address this problem, conductive additives like amorphous carbon [7], graphene [8], carbon nanotubes (CNT) [9] and conducting polymers [8,10] were added to different polymorphs of TiO_2. Since addition of large amounts of conductive additives contributes little to capacitance of the device, this is not a favorable option. Furthermore, some carbon materials like CNT and graphene are fairly expensive to produce.

To overcome this issue, oxygen defects in the metal oxide lattice structure can be introduced, as they have been reported to improve the conductivity of the material by reducing the bandgap [11]. For instance, yellowish and black TiO_2 nanoparticles after hydrogen treatment showed a significant increase in capacity in lithium-ion batteries [12,13]. However, the origin of this improved electrochemical activity has not been fully understood and even the increase of capacitance has not been supported with sufficient evidence.

Metal oxides (e.g., MnO_2, RuO_2, Nb_2O_5, etc.) are well-known pseudocapacitive materials, which have been studied in various configurations [2,14]. However, only a few reports are available on the TiO_2(B) phase as a lithium insertion electrode [15–17], and particularly, the effect of hydrogenation of TiO_2(B) on electrochemical performance

* Corresponding author. Tel.: +1 215 895 6446; fax: +1 215 895 1934.
** Corresponding author. Tel.: +82 42 350 3940; fax: +82 42 350 3910.
E-mail addresses: jaewlee@kaist.ac.kr (J.W. Lee), gogotsi@drexel.edu (Y. Gogotsi).
[1] These authors equally contributed to this work.
[2] Present address: Department of Materials Engineering, Auburn University, Auburn, AL 36849, United States.

http://dx.doi.org/10.1016/j.elecom.2015.09.004
1388-2481/

for lithium-ion capacitor is not well studied. Recently, partially reduced oxides have shown improvement in photocatalytic activity and electrochemical properties in both lithium-ion batteries and supercapacitors [11,12]. In all cases, the improved electrochemical performance of the oxides was attributed to the defect-induced conductivity due to decrease in the bandgap. Hydrogen plasma treatment [18], sodium borohydride ($NaBH_4$) reduction [19], vacuum annealing [20] and heat treatment under H_2 at atmospheric pressure [21] have been used to make oxygen-deficient oxides.

Herein, one-dimensional TiO_2(B) nanowires were synthesized via hydrothermal method followed by heat treatment under hydrogen gas for the introduction of Ti^{3+} to create oxygen deficiency. The resulting TiO_2 NW and H_2-TiO_2 NW were tested in organic electrolyte as an anode for LICs. Electrochemical performance is compared with other hydrogenated oxides and the challenges to achieve higher capacity via the hydrogenation method are elaborated.

2. Experimental

2.1. TiO_2 NW/H_2-TiO_2 NW synthesis

3.7 g of anatase TiO_2 (15 nm, Alfa Aesar) nanoparticles were stirred with 20 ml of 15 M NaOH (Sigma) for 1 h. The suspension was put into a Teflon-lined stainless steel autoclave and heated at 180 °C for 72 h, followed by washing with 0.1 M HCl until the supernatant became neutral. Dried powder was heated to 450 °C for 5 h in air to produce TiO_2(B) phase nanowires (TiO_2 NW). Heating up to 4 h at 500 °C under hydrogen atmosphere (Ar—10% H_2), following the process conditions reported in the literature [12,21–23] led to hydrogenated TiO_2 NW (H_2-TiO_2 NW).

2.2. Electrode preparation

The slurry was made by mixing 80 wt% of TiO_2 NW or H_2-TiO_2 NW with 10 wt% polyvinylidene fluoride (Alfa Aesar, Ward Hill, USA) binder and 10 wt% carbon black (Alfa Aesar, Ward Hill, USA) in 1-methyl-2-pyrrolidinone (Alfa Aesar, Ward Hill, USA). A 200 μm thick coating was deposited on copper foil using a doctor blade and dried overnight resulting in ~80 μm thick electrodes. The coated dried foil was punched into 5 mm diameter disks, which were used for the electrochemical testing.

2.3. Electrochemical setup

The electrodes were tested in a three-electrode configuration using a Swagelok® cell with TiO_2(B) NW or H_2-TiO_2(B) NW as the working electrode, activated carbon as a counter electrode and silver (Ag) wire as a reference electrode. Two layers of Celgard separator were used and tests were conducted in 1 M solution of lithium perchlorate (Sigma) in 1:1 volume ratio of ethylene carbonate (Sigma) and diethyl carbonate (Sigma) electrolyte. Cyclic voltammetry (CV) was performed on a potentiostat (VMP3, Biologic, France) at different scan rates from 1 to 20 mV/s. Electrochemical impedance spectroscopy (EIS) was run in the frequency range of 200 kHz to 10 mHz at a sine wave signal amplitude of +/− 10 mV centered at 0 V vs. open circuit potential.

The specific capacitance (C_{sp}) was calculated according to Eq. (1):

$$C_{sp} = \frac{1}{\Delta E}\frac{\int i\,dV}{\nu m} \tag{1}$$

where, ΔE is the voltage window, i is the discharge current, V is the voltage, v is the sweep rate, and m is the mass of active material in one electrode. The energy density and power density were obtained from Eq. (2):

$$E = \frac{1}{2}CV^2 \qquad P = \frac{E}{t} \tag{2}$$

where, E, C, V, P and t represent energy density, capacitance, voltage window, power density, and discharge time, respectively.

2.4. Characterization

The morphology of the samples was characterized using a transmission electron microscope (TEM) (JEOL JEM-2100, Japan) with an accelerating voltage of 200 kV. The TEM samples were prepared by placing several drops of the sample dispersion in ethanol onto a copper grid and drying in air. The x-ray diffraction (XRD) analysis was performed on a powder diffractometer (Rigaku Smart Lab, USA) with Cu Kα radiation. To investigate the changes in surface area, gas sorption analysis was carried out using quadrosorb gas sorption instrument (Qunatachrome, USA) using N_2 gas adsorbate at −196 °C. XPS measurements were done using a Physical Electronics VersaProbe 5000 instrument of 100 μm monochromatic Al-kα X-ray. Photoelectrons were collected by a 180° hemispherical electron energy analyzer. Samples were analyzed at a 45° takeoff angle between the sample surface and the path to the analyzer. High-resolution spectra were taken at a pass energy of 23.5 eV, with a step size of 0.05 eV. The spectra were taken after the sample was sputtered with an Ar beam operating at 4 kV and 150 μA for 15 min. All binding energies were referenced to that of free carbon at 284.5 eV. The quantification and peak fitting of the spectra were performed using CasaXPS Version 2.3.16 RP 1.6. Prior to peak fitting, the background contributions were subtracted using a Shirley function. For all $2p_{3/2}$ and $2p_{1/2}$ components, the intensity ratios of the peaks were constrained to be 2:1.

3. Results and discussions

Fig. 1 presents a schematic of the synthesis process. Hydrothermal synthesis was considered because it is simple, relatively inexpensive and produces gram-scale amounts of the material [24,25]. The absence of the anatase peaks from the x-ray diffraction (XRD) pattern (Fig. 2a) confirmed the conversion of the TiO_2 anatase phase into TiO_2 bronze and the XRD pattern was found similar to previous reports [26]. As-synthesized NW were 20–40 nm in diameter and 1–5 μm in length

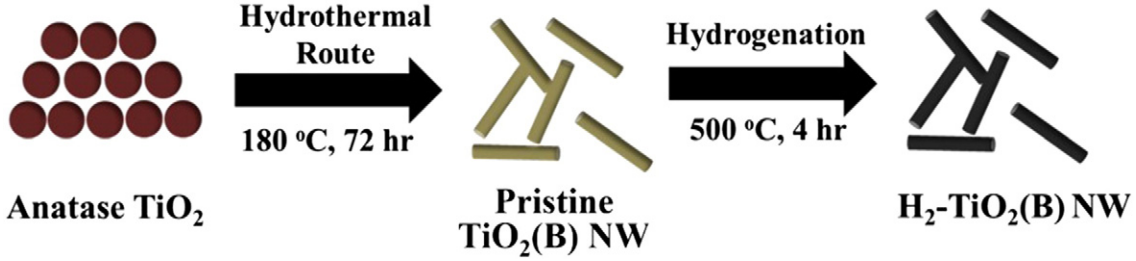

Fig. 1. Schematic presentation of the hydrothermal synthesis and hydrogenation of TiO_2(B) NW.

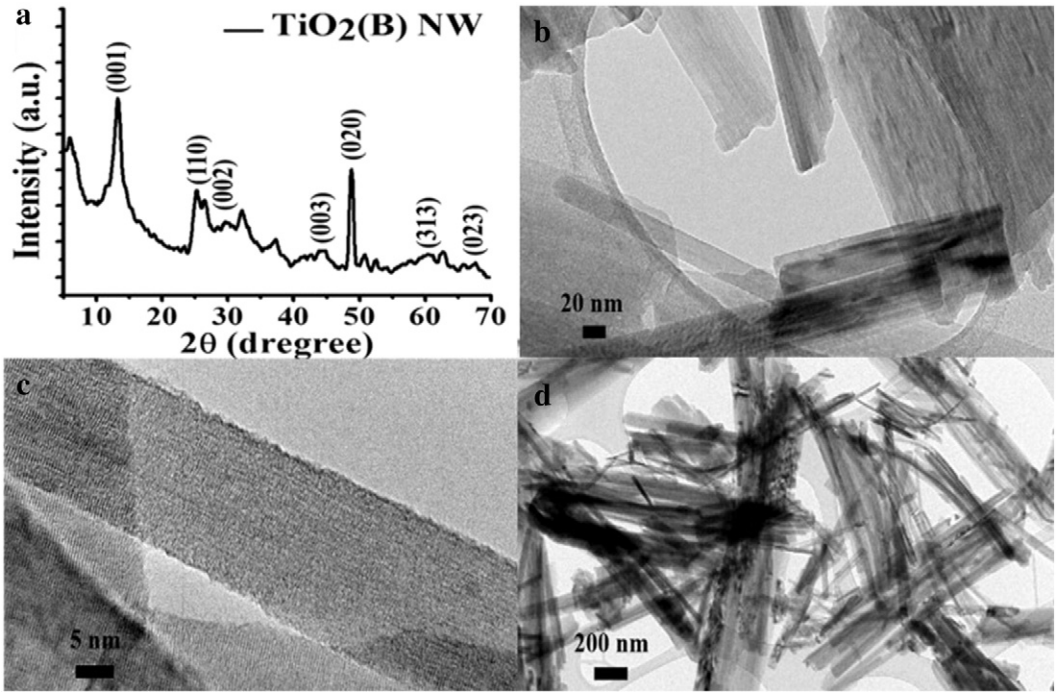

Fig. 2. (a) X-ray diffraction pattern of TiO_2(B) NW, (b–d) transmission electron microscopy (TEM) images of hydrothermally synthesized TiO_2(B) NW.

(Fig. 2b-d)—thinner and longer compared to the previous reports (100 nm thickness and 1 μm length [15]), most likely due to the use of a nanometer scale initial precursor. Therefore, such ultra-fine NW offer large number of active sites for lithium insertion and short diffusion pathways for the improved electrochemical performance. Moreover, the open-structure NW morphology of TiO_2 (B) may be favorable for Li^+ intercalation. The surface area of H_2-TiO_2(B) NW was found to be 9.5 m^2/g. Therefore, it is believed that surface area doesn't have large impact on its electrochemical performance.

We have performed XPS analysis on our pristine and hydrogenated samples (Fig. 3). For example, the oxygen content of pristine and hydrogenated TiO_2(B) NW is 67.0 and 66.6 at.%. Also, the relative concentrations of Ti^{3+}/Ti^{2+} of TiO_2(B) NW and hydrogenated TiO_2(B) NW were 3.1 and 2.7.

Cyclic voltammograms (CVs) at various scan rates were acquired in the voltage window of 2.1 V (Fig. 4). Two broad redox peaks appeared at about −1.5 V and −2.0 V, which correspond to the following lithium insertion/extraction processes:

$$TiO_2(B) + xLi \leftrightarrow LixTiO_2(B). \quad (3)$$

After hydrogenation, these peaks shifted toward higher potentials (−1.3 V and −1.7 V) and separation between the peaks decreased, which may indicate a change in the electronic structure of the TiO_2(B) NW. The CV shape of H_2-TiO_2 NW appeared wider (more capacitive) than pristine TiO_2 NW (Fig. 4a–b), most likely due to the improved conductivity and change in the oxidation state of the Ti, as shown by in-situ x-ray absorption spectroscopy study [27]. However, in order to

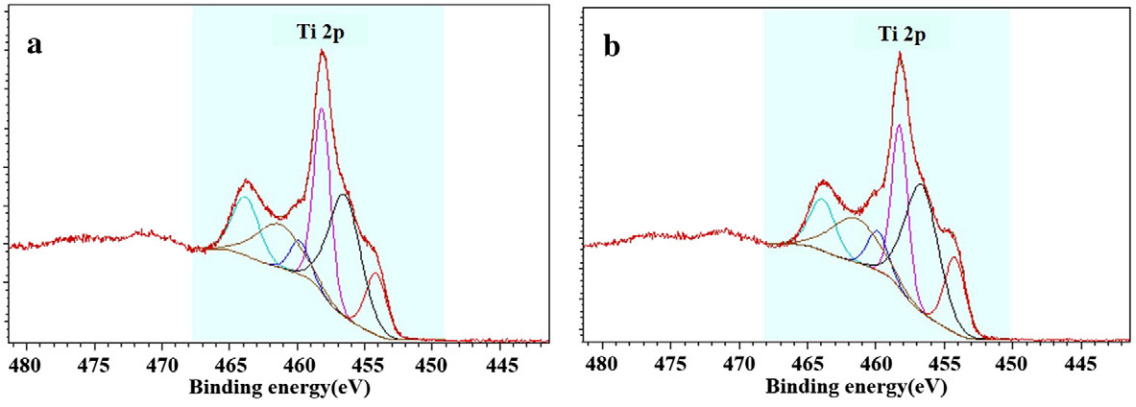

Region	BE [eV]	Fraction	Assigned to
Ti $2p_{3/2}$ ($2p_{1/2}$)	454.2 (459.8)	0.15	Ti^{+2}
	456.5 (461.4)	0.47	Ti^{+3}
	458.2 (463.8)	0.38	TiO_2

Region	BE [eV]	Fraction	Assigned to
Ti $2p_{3/2}$ ($2p_{1/2}$)	454.2 (459.9)	0.18	Ti^{+2}
	456.6 (461.5)	0.50	Ti^{+3}
	458.2 (463.8)	0.32	TiO_2

Fig. 3. (a) XPS spectra of TiO_2(B) NW and (b) H_2-TiO_2(B) NW after sputtering.

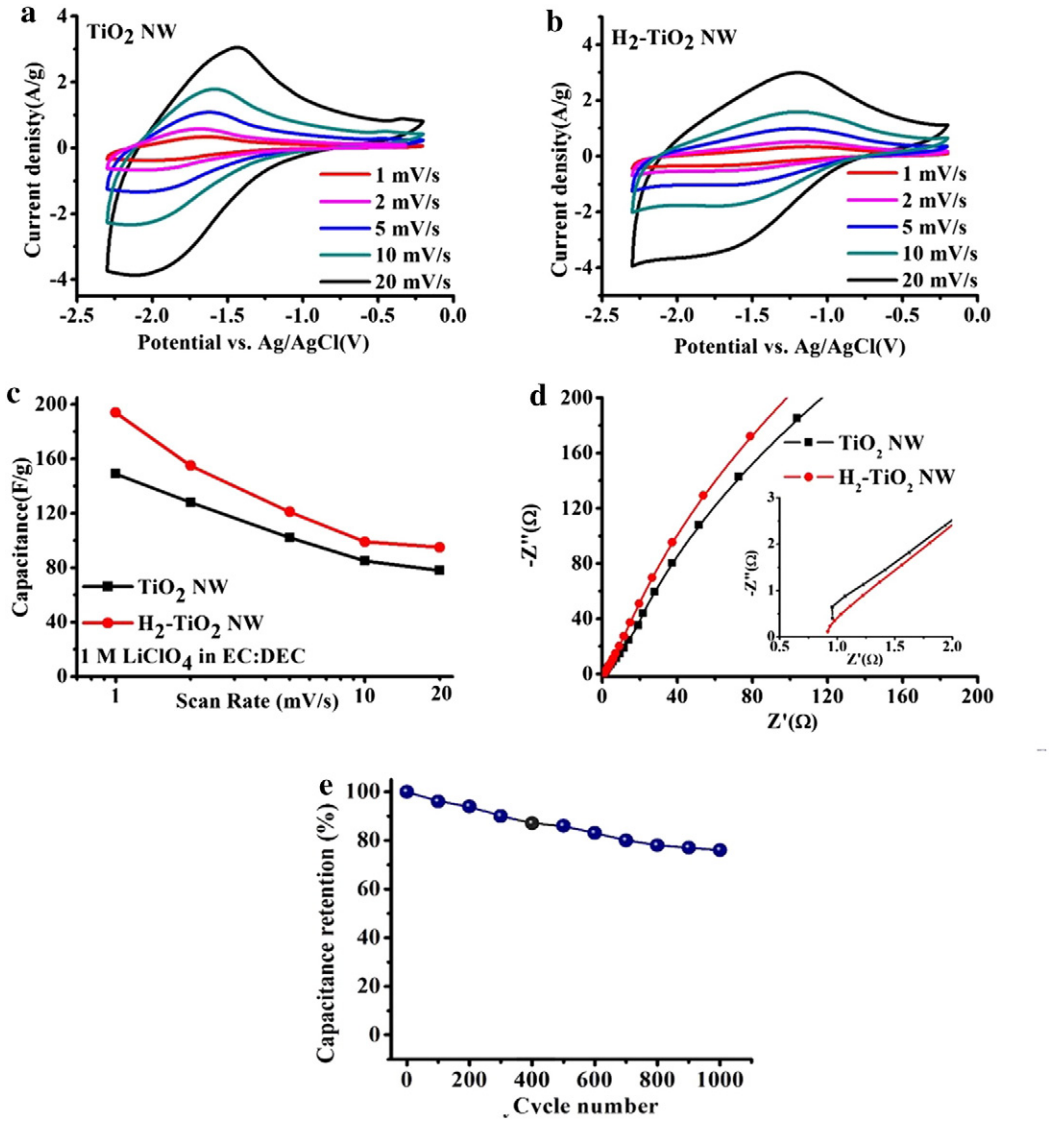

Fig. 4. (a) Cyclic voltammograms of TiO_2(B) NW, (b) CVs of H_2-TiO_2(B) NW, (c) corresponding rate performance, (d) Nyqiust plots of TiO_2 (B) NW and H_2-TiO_2(B) NW, and (e) cyclic stability up to 1000 cycles of H_2-TiO_2(B) NW.

better understand the hydrogenation induced changes in the oxidation state of Ti and to correlate such changes with the electrochemical performance, further in-situ studies are required, as conducted on other pseudocapacitive materials [27–29]. The capacitance of H_2-TiO_2 NW was found to be 194 F/g at the lowest scan rate of 1 mV/s—30% higher than pristine TiO_2 NW at the same scan rate (148 F/g, Fig. 4c). It is worth noting that our as-synthesized TiO_2(B) NW electrodes demonstrated a higher capacitance than in various previous reports [15,17,30]. For instance, TiO_2(B) NW@activated carbon yielded 52 F/g at 0.1 A/g [15] and TiO_2-reduced graphene oxide@activated carbon showed 89 F/g at 2 A/g [30]. Also, our 80 μm titania electrodes (similar to commercial LIC electrodes in thickness) showed a much higher capacitance even compared to a much thinner nanometer-scale TiO_2 film (150 nm) [4]. Likely, thinner NW, shorter diffusion paths and the increased surface area lead to the higher capacitance.

Although the as-synthesized TiO_2(B) NW outperformed previous reports, we did not observe a dramatic improvement in the capacitance after hydrogenation of the TiO_2(B) NW, opposed to some other hydrogenated oxides [21,31–33]. It is reported that hydrogenation induced oxygen defects change the electronic band structure of the oxides, which tune the optical and charge transfer properties of the oxide-based electrodes. This, in turn, significantly improves electrochemical activity of the material. It is most likely that the change in the bandgap will enhance the photocatalytic properties, which are strongly dependent on bandgap variation of oxide semiconductors after hydrogenation [11,18]. However, the relationship between oxygen defects induced by hydrogenation and their effect on the conductivity and capacitance needs deeper understanding.

Nyquist plots measured by the impedance spectroscopy (Fig. 4d) of both electrodes showed a negligible semicircle and very small charge transfer resistance (R_{ct}). The ohmic resistance (R_Ω), of both electrodes was comparable (0.93 Ω). Although, both electrodes appeared capacitive in the low frequency regime, the Nyquist plot of H_2-TiO_2 NW appeared more capacitive than pristine electrodes. This is most likely due to the improved charge percolation and low electronic resistance in the hydrogenated electrode [34].

Rate performance of both electrodes shows that H_2-TiO_2 NW exhibits a higher capacitance across the entire range of sweep rates (1–20 mV/s). High cycling stability is critical for the lithium ion battery electrodes experiencing intercalation/deintercalation. The cycling stability was tested at 2 A/g for 1000 cycles. The H_2-TiO_2 NW electrode showed a stable cycling behavior with 80% capacitance retention after 1000 cycles (Fig. 4e).

To conclude, we have synthesized TiO_2(B) NW with diameters between 20–40 nm and 1–5 μm in length. As-synthesized TiO_2(B) NW exhibited excellent charge storage capacity of 148 F/g in organic electrolyte, which is attributed to the fine NW morphology, good conductivity and short diffusional pathways. The hydrogenation led to ~30% increase in capacitance to 194 F/g. The corresponding energy density was 30 Wh/kg—higher than pristine TiO_2(B) NW. Although hydrogenation improved the charge storage capacity, we did not observe a dramatic increase in capacitance after the hydrogenation process, which was predicted in some studies [21,31–33]. We emphasize that more theoretical and experimental work directed toward understanding the relationship between concentration of the oxygen vacancies, conductivity and hydrogenation conditions of titania is needed to further improve energy storage.

Conflict of interest

The authors declare no competing financial interests.

Acknowledgments

This work was supported by the U.S. Department of Energy, Office of Electricity, Energy Storage Systems Program, through Sandia National Laboratory. The authors are thankful to Dr. Alexey Glushenkov for TEM analysis, Dr. Babak Anasori and Sankalp Kota for XRD analysis and Joseph Halim for XPS analysis and valuable discussions. M. Boota, M. Beidaghi and K.V. Aken were supported by the Fluid Interface Reactions, Structures and Transport (FIRST) Center, an Energy Frontier Research Center funded by the U.S. Department of Energy, Office of Science, Basic Energy Sciences. A. Byeon acknowledges support from the BK-21 Plus program and the Korea CCS R & D program funded by the Ministry of Science, ICT, and Future Planning (NRF-2014M1A8A1049297).

References

[1] P. Simon, Y. Gogotsi, Materials for electrochemical capacitors, Nat. Mater. 7 (2008) 845–854, http://dx.doi.org/10.1038/nmat2297.
[2] V. Augustyn, P. Simon, B. Dunn, Pseudocapacitive oxide materials for high-rate electrochemical energy storage, Energy Environ. Sci. 7 (2014) 1597–1614, http://dx.doi.org/10.1039/c3ee44164d.
[3] M. Boota, K.B. Hatzell, E.C. Kumbur, Y. Gogotsi, Towards high-energy-density pseudocapacitive flowable electrodes by the incorporation of hydroquinone, ChemSusChem 8 (2015) 835–843, http://dx.doi.org/10.1002/cssc.201402985.
[4] T. Brezesinski, J. Wang, J. Polleux, B. Dunn, S.H. Tolbert, Templated nanocrystal-based porous TiO_2 films for next-generation electrochemical capacitors, J. Am. Chem. Soc. 131 (2009) 1802–1809, http://dx.doi.org/10.1021/ja8057309.
[5] K. Naoi, S. Ishimoto, J. Miyamoto, W. Naoi, Second generation "nanohybrid supercapacitor": evolution of capacitive energy storage devices, Energy Environ. Sci. 5 (2012) 9363–9373, http://dx.doi.org/10.1039/c2ee21675b.
[6] A.G. Dylla, G. Henkelman, K.J. Stevenson, Lithium insertion in nanostructured TiO_2(B) architectures, Acc. Chem. Res. 46 (2013) 1104–1112, http://dx.doi.org/10.1021/ar300176y.
[7] T. Xia, W. Zhang, Z. Wang, Y. Zhang, X. Song, J. Murowchick, et al., Amorphous carbon-coated TiO_2 nanocrystals for improved lithium-ion battery and photocatalytic performance, Nano Energy 6 (2014) 109–118, http://dx.doi.org/10.1016/j.nanoen.2014.03.012.
[8] L. Jiang, X. Lu, C. Xie, G. Wan, H. Zhang, T. Youhong, Flexible, free-standing TiO_2–graphene–polypyrrole composite films as electrodes for supercapacitors, J. Phys. Chem. C 119 (2015) 3903–3910, http://dx.doi.org/10.1021/jp511022z.
[9] K. Naoi, W. Naoi, S. Aoyagi, J.-I. Miyamoto, T. Kamino, New generation "nanohybrid supercapacitor", Acc. Chem. Res. 46 (2013) 1075–1083, http://dx.doi.org/10.1021/ar200308h.
[10] P.M. Dziewoński, M. Grzeszczuk, Towards TiO_2-conducting polymer hybrid materials for lithium ion batteries, Electrochim. Acta 55 (2010) 3336–3347, http://dx.doi.org/10.1016/j.electacta.2010.01.043.
[11] G. Wang, Y. Ling, Y. Li, Oxygen-deficient metal oxide nanostructures for photoelectrochemical water oxidation and other applications, Nanoscale 4 (2012) 6682–6691, http://dx.doi.org/10.1039/C2NR32222F.
[12] J.-Y. Shin, J.H. Joo, D. Samuelis, J. Maier, Oxygen-deficient $TiO_{2-\delta}$ nanoparticles via hydrogen reduction for high rate capability lithium batteries, Chem. Mater. 24 (2012) 543–551, http://dx.doi.org/10.1021/cm2031009.
[13] Y. Yan, B. Hao, D. Wang, G. Chen, E. Markweg, A. Albrecht, et al., Understanding the fast lithium storage performance of hydrogenated TiO_2 nanoparticles, J. Mater. Chem. A. 1 (2013) 14507–14513, http://dx.doi.org/10.1039/C3TA13491A.
[14] V. Augustyn, J. Come, M.A. Lowe, J.W. Kim, P.-L. Taberna, S.H. Tolbert, et al., High-rate electrochemical energy storage through Li^+ intercalation pseudocapacitance, Nat. Mater. 12 (2013) 518–522, http://dx.doi.org/10.1038/nmat3601.
[15] V. Aravindan, N. Shubha, W.C. Ling, S. Madhavi, Constructing high energy density non-aqueous Li-ion capacitors using monoclinic TiO_2-B nanorods as insertion host, J. Mater. Chem. A. 1 (2013) 6145–6151, http://dx.doi.org/10.1039/C3TA11103B.
[16] H. Wang, C. Guan, X. Wang, H.J. Fan, A high energy and power Li-ion capacitor based on a TiO_2 nanobelt array anode and a graphene hydrogel cathode, Small 11 (2015) 1470–1477, http://dx.doi.org/10.1002/smll.201402620.
[17] Q. Wang, Z.H. Wen, J.H. Li, A hybrid supercapacitor fabricated with a carbon nanotube cathode and a TiO_2-B nanowire anode, Adv. Funct. Mater. 16 (2006) 2141–2146, http://dx.doi.org/10.1002/adfm.200500937.
[18] Y. Yan, M. Han, A. Konkin, T. Koppe, D. Wang, T. Andreu, et al., Slightly hydrogenated TiO_2 with enhanced photocatalytic performance, J. Mater. Chem. A. 2 (2014) 12708–12716, http://dx.doi.org/10.1039/C4TA02192D.
[19] W. Fang, M. Xing, J. Zhang, A new approach to prepare Ti^{3+} self-doped TiO_2 via $NaBH_4$ reduction and hydrochloric acid treatment, Appl. Catal. B Environ. 160–161 (2014) 240–246, http://dx.doi.org/10.1016/j.apcatb.2014.05.031.
[20] M. Xing, J. Zhang, B. Qiu, B. Tian, M. Anpo, M. Che, A brown mesoporous TiO_{2-x}/MCF composite with an extremely high quantum yield of solar energy photocatalysis for H_2 evolution, Small 11 (2015) 1920–1929, http://dx.doi.org/10.1002/smll.201403056.
[21] X. Lu, G. Wang, T. Zhai, M. Yu, J. Gan, Y. Tong, et al., Hydrogenated TiO_2 nanotube arrays for supercapacitors, Nano Lett. 12 (2012) 1690–1696, http://dx.doi.org/10.1021/nl300173j.
[22] A. Naldoni, M. Allieta, S. Santangelo, M. Marelli, F. Fabbri, S. Cappelli, et al., Effect of nature and location of defects on bandgap narrowing in black TiO_2 nanoparticles, J. Am. Chem. Soc. 134 (2012) 7600–7603, http://dx.doi.org/10.1021/ja3012676.
[23] G. Wang, H. Wang, Y. Ling, Y. Tang, X. Yang, R.C. Fitzmorris, et al., Hydrogen-treated TiO_2 nanowire arrays for photoelectrochemical water splitting, Nano Lett. 11 (2011) 3026–3033, http://dx.doi.org/10.1021/nl201766h.
[24] Y. Gogotsi, K.G. Nickel, D. Bahloul-Hourlier, T. Merle-Mejean, G.E. Khomenko, K.P. Skjerlie, Structure of carbon produced by hydrothermal treatment of β-SiC powder, J. Mater. Chem. 6 (1996) 595–604, http://dx.doi.org/10.1039/jm9960600595.
[25] M. Boota, K.B. Hatzell, M. Alhabeb, E.C. Kumbur, Y. Gogotsi, Graphene-containing flowable electrodes for capacitive energy storage, Carbon N. Y. 92 (2015) 142–149, http://dx.doi.org/10.1016/j.carbon.2015.04.020.
[26] V. Etacheri, Y. Kuo, A. Van der Ven, B.M. Bartlett, Mesoporous TiO_2-B microflowers composed of (1 $\bar{1}$ 0) facet-exposed nanosheets for fast reversible lithium-ion storage, J. Mater. Chem. A. 1 (2013) 12028–12032, http://dx.doi.org/10.1039/c3ta12920a.
[27] M.R. Lukatskaya, S.-M. Bak, X. Yu, X.-Q. Yang, M.W. Barsoum, Y. Gogotsi, Probing the mechanism of high capacitance in 2D titanium carbide using in situ X-ray absorption spectroscopy, Adv. Energy Mater. 5 (2015) 1500589, http://dx.doi.org/10.1002/aenm.201500589.
[28] J.-K. Chang, M.-T. Lee, W.-T. Tsai, In situ Mn K-edge X-ray absorption spectroscopic studies of anodically deposited manganese oxide with relevance to supercapacitor applications, J. Power Sources 166 (2007) 590–594, http://dx.doi.org/10.1016/j.jpowsour.2007.01.036.
[29] M. Toupin, T. Brousse, D. Bélanger, Charge storage mechanism of MnO_2 electrode used in aqueous electrochemical capacitor, Chem. Mater. 16 (2004) 3184–3190, http://dx.doi.org/10.1021/cm049649j.
[30] H. Kim, M.-Y. Cho, M.-H. Kim, K.-Y. Park, H. Gwon, Y. Lee, et al., A novel high-energy hybrid supercapacitor with an anatase TiO_2-reduced graphene oxide anode and an activated carbon cathode, Adv. Energy Mater. 3 (2013) 1500–1506, http://dx.doi.org/10.1002/aenm.201300467.
[31] H. Wu, C. Xu, J. Xu, L. Lu, Z. Fan, X. Chen, et al., Enhanced supercapacitance in anodic TiO_2 nanotube films by hydrogen plasma treatment, Nanotechnology 24 (2013) 455401, http://dx.doi.org/10.1088/0957-4484/24/45/455401.
[32] Y. Wang, T. Zhou, K. Jiang, P. Da, Z. Peng, J. Tang, et al., Reduced mesoporous Co_3O_4 nanowires as efficient water oxidation electrocatalysts and supercapacitor electrodes, Adv. Energy Mater. 4 (2014) 1400696, http://dx.doi.org/10.1002/aenm.201400696.
[33] T. Zhai, S. Xie, M. Yu, P. Fang, C. Liang, X. Lu, et al., Oxygen vacancies enhancing capacitive properties of MnO_2 nanorods for wearable asymmetric supercapacitors, Nano Energy 8 (2014) 255–263, http://dx.doi.org/10.1016/j.nanoen.2014.06.013.
[34] H.-M. Cho, W.-S. Choi, J.-Y. Go, S.-E. Bae, H.-C. Shin, A study on time-dependent low temperature power performance of a lithium-ion battery, J. Power Sources 198 (2012) 273–280, http://dx.doi.org/10.1016/j.jpowsour.2011.09.111.